View metadata, citation and similar papers at core.ac.uk

brought to you by CORE

provided by University of Queensland eSpace

A morphology independent approach for identifying dividing adult neural stem cells in the mouse hippocampus

Lachlan Harris[1], Oressia Zalucki[1], Sabrina Oishi[1], Thomas H. Burne[3,4], Dhanisha J. Jhaveri[2,3] and Michael Piper[1, 3]

[1]The School of Biomedical Sciences, The University of Queensland, Brisbane, QLD, Australia 4072.

[2] Mater Research Institute, The University of Queensland, QLD 4102, Australia.

[3]Queensland Brain Institute, The University of Queensland, Brisbane, Australia 4072.

[4]Queensland Centre for Mental Health Research, The Park Centre for Mental Health, Wacol, QLD, Australia 4076.

*Correspondence to: Michael Piper
The School of Biomedical Sciences
The University of Queensland
Brisbane, 4072, Australia
Tel: (+61) 7 3365 4484
Fax: (+61) 7 3365 1766
E-mail: m.piper@uq.edu.au

Abstract

Background

Type 1 adult hippocampal neural stem cells (AH-NSCs) continue to generate neurons throughout life, albeit at a very low rate. The relative quiescence of this population of cells has led to many studies investigating factors that may increase their division. Current methods of identifying dividing AH-NSCs *in vivo* require the identification and tracing of radial processes back to nuclei within the subgranular zone. However, caveats to this approach include the time-intensive nature of identifying AH-NSCs with such a process, as well as the fact that this approach ignores the relatively more active population of horizontally oriented AH-NSCs that also reside in the subgranular zone.

Results

Here, we describe, and then verify using *Hes5*::GFP mice, that labelling for the cell-cycle marker Ki67, and selection against the intermediate progenitor cell marker TBR2 ($Ki67^{+ve}$; $TBR2^{-ve}$ nuclei) is sufficient to identify dividing horizontally- and radially-orientated AH-NSCs in the adult mouse hippocampus.

Conclusion

These findings provide a simple and accurate way to quantify dividing AH-NSCs in vivo using a morphology independent approach that will facilitate studies into neurogenesis within the hippocampal stem cell niche of the adult brain.

Introduction

The continued generation of dentate granule neurons from AH-NSCs is important for multiple cognitive processes, including learning (Akers et al., 2014; Goncalves et al., 2016) and mood regulation in mice (Yun et al., 2016). The level of adult hippocampal neurogenesis in humans is comparable to that in mice, suggesting that ongoing neurogenesis is functionally important for both species (Spalding et al., 2013; Bergmann et al., 2015; Ernst and Frisen, 2015). As a consequence of this, therapies are being developed that aim to specifically increase the levels of hippocampal neurogenesis to circumvent disorders such as depression, where neurogenesis is reduced (Harris et al., 2016b; Yun et al., 2016).

There are three major cell types within the neurogenic lineage of the adult mouse hippocampus (reviewed in (Goncalves et al., 2016)). These are the AH-NSCs (Type 1 cells), most of which are quiescent, the transient but highly proliferative intermediate progenitors (IPs or Type 2 cells), and finally neuroblasts (Type 3 cells). These cell types are defined by their relative division capacity, lineage potential, and expression of certain markers (von Bohlen und Halbach, 2011). Despite the intense interest in neurogenesis in the adult brain, one of the major challenges in the field is to clearly define these cellular populations, and particularly challenging in this respect is unequivocally identifying dividing AH-NSCs *in vivo*. The ability to accurately identify dividing AH-NSCs is crucial to determine the relative rates of quiescence or division among this population. A recent study using novel cell sorting protocol identified and purified to homogeneity almost the entire population of neurosphere-forming precursors comprising both dividing and quiescent AH-NSCs (Jhaveri et al., 2015), however this approach is not easily applied to the histological identification of these cells. In most studies, the histological criteria used to identify dividing AH-NSCs *in vivo* involve linking a radial process, stained for Glial Fibrillary Acidic Protein (GFAP), Nestin, Brain Lipid-binding Protein (BLBP) or Epidermal Growth Factor Receptor (EGFR) expression, back to a nucleus within the subgranular zone (SGZ) and determining whether the nucleus is positive for a cell-cycle marker, such as Ki67 (von Bohlen und Halbach, 2011; Hussaini et al., 2013; Jhaveri et al., 2015). Despite the large number of studies to have utilised this approach, there are a number of inherent difficulties evident with this paradigm for identifying dividing AH-NSCs.

Foremost among the problems associated with tracing a radial process is that the current approach ignores a population of horizontally oriented cells that are putative NSCs (Lugert et al., 2010). These putative horizontal NSCs (not to be confused with IPs, which are also horizontal dividing precursors) have different characteristics from their radial NSC counterparts. For example, horizontal AH-NSCs divide more frequently, and their numbers change more acutely in response to age or exercise (Lugert et al., 2010). This shortcoming implies that the many studies that have not analysed this cellular population may have underrepresented the number of dividing AH-NSCs present. While further work, such as lineage tracing, needs to be performed to confirm these horizontal cells as *bona fide* NSCs with the capacity to generate neurons and/or glia, an inclusive approach that accounts for the potential morphological heterogeneity of AH-NSCs should be developed. The second problem with the existing radial identification approach is that it is potentially inaccurate and extremely time-consuming. Dividing AH-NSCs and intermediate progenitors (IPs) are frequently found together in clusters (Hodge et al., 2008), and therefore it becomes difficult to determine to which cell a radial AH-NSC process is linked. Finally, there is a lack of standardisation as to which radial markers are appropriate to use when identifying dividing AH-NSCs, demonstrated by the variety employed in the following studies (Gulbins et al., 2013; Li et al., 2013; Martynoga et al., 2013; Andersen et al., 2014; Kandasamy et al., 2014; Andreu et al., 2015; Nicola et al., 2015; Yousef et al., 2015). Together, these issues pose great challenges to the interpretation and comparison of the many studies in this field.

To address these issues, we developed a morphology independent approach for identifying dividing AH-NSCs. Our method is based solely on the exclusion of the IP marker TBR2 (Hodge et al., 2008; Hodge et al., 2012). We found that Ki67^{+ve}; TBR2^{-ve} cells have large nuclei, express higher levels of SOX2 and are *Hes5*::GFP^{+ve}. Most importantly, we verified in the notch reporter *Hes5*::GFP mouse strain (Jhaveri et al., 2010; Lugert et al., 2010) that a subset of these cells also have a horizontal GFP^{+ve} morphology, consistent with the description of horizontal NSCs by Lugert and colleagues (2010). The approach outlined here is accurate, fast and accounts for the heterogeneous morphology of AH-NSCs, representing a significant advance on previous approaches used to identify and quantify this population *in vivo*.

Results

Selecting a nuclear marker for dividing AH-NSCs

To develop a morphology independent approach for identifying dividing AH-NSCs we first needed to identify a suitable nuclear protein to use as a marker. As no protein has been identified that alone specifically labels this population, we sought to identify a proxy marker, which could then be used in conjunction with other proteins to identify AH-NSCs. Two criteria were assessed; first, the percentage of dividing AH-NSCs that are labelled by the nuclear protein (penetrance), and, secondly, the other cell types that express the protein (specificity).

Two proteins satisfied these criteria and appeared to be reasonable candidates, namely Achaete-scute like 1 (ASCL1) and Ki67. The basic helix-loop-helix protein ASCL1 is a proneural factor required for AH-NSCs to enter the cell-cycle (Andersen et al., 2014; Urban et al., 2016). Because ASCL1 protein is not expressed by quiescent AH-NSCs and labels only a fraction of IPs (Kim et al., 2011), it displays good specificity. However, ASCL1 is not a completely penetrant marker, as it expressed by only by one-third of dividing AH-NSCs (Andersen et al., 2014). Moreover, ASCL1 also has functions in fate specification and differentiation in the embryonic nervous system (Castro et al., 2011; Guillemot and Hassan, 2016), and when ectopically expressed in the adult hippocampus, it leads to aberrant formation of oligodendrocytes (Braun et al., 2015). Therefore, in mouse models where fate specification is altered it may no longer serve as a reliable readout of AH-NSC division.

In contrast, Ki67 appears to be a more suitable choice for a proxy marker of AH-NSC division. For example, Ki67 is expressed throughout the cell cycle and therefore should label all dividing AH-NSCs (high penetrance) (Gerdes et al. 1983; Endl and Gerdes 2000). In the SGZ, it is expressed only by dividing AH-NSCs, dividing IPs and dividing neuroblasts and thereby also displays reasonable specificity (Scholzen and Gerdes, 2000). Moreover, because the function of Ki67 is restricted to chromatin organisation during cell division (Cuylen et al., 2016) it serves as a direct readout of division, which is unlikely to be altered in mouse models where fate specification is altered. Consequently, we chose to investigate whether Ki67, in combination with

other markers, could be used to specifically identify dividing AH-NSCs in the hippocampus.

Negative selection against TBR2 is sufficient to exclude dividing IPCs and neuroblasts

To distinguish between dividing nuclei ($Ki67^{+ve}$) that are AH-NSCs, and those that are dividing IPs or neuroblasts, we co-stained 12-16 week-old C57BL/6J mice with Ki67, the IP marker TBR2 and the neuroblast marker DCX (Figure 1A, B). We hypothesised that the exclusion of $TBR2^{+ve}$ and DCX^{+ve} cells would leave a population of $Ki67^{+ve}$; $TBR2^{-ve}$; DCX^{-ve} cells within the SGZ that would comprise the dividing AH-NSC pool. To assess the plausibility of this experimental design, we first examined the percentage of IPs and neuroblasts that expressed Ki67. We focussed our analysis to the SGZ specifically (see Experimental Procedures). Consistent with previous reports we found that the majority of $TBR2^{+ve}$ cells were labelled with Ki67 (83.1%, Figure 1C, D) (Hodge et al., 2008), while only 13.9% of DCX^{+ve} cells were labelled with Ki67 (Figure 1E, F). At this stage we also made an important observation. All dividing DCX^{+ve} neuroblasts had an immature IP-like morphology and expressed TBR2 (Figure 1F). Because all dividing neuroblasts also expressed TBR2, this led us to posit that selection against TBR2 alone should be sufficient to identify dividing AH-NSCs.

$Ki67^{+ve}$; $TBR2^{-ve}$ cells are dividing AH-NSCs

To assess whether the dividing $TBR2^{-ve}$ cells were AH-NSCs we examined three parameters. First, we measured the relative expression of SOX2. In AH-NSCs the transcription factor SOX2 is down regulated as these cells differentiate, so that AH-NSCs express relatively higher levels of SOX2 than IPs (Hodge et al., 2012; Shin et al., 2015). We stained adult mouse hippocampal sections for Ki67, TBR2 and SOX2. Supporting their identity as AH-NSCs, dividing $TBR2^{-ve}$ cells had a much higher expression of SOX2 than dividing $TBR2^{+ve}$ cells (Figure 2A, B; $P < 0.001$). Importantly, SOX2 expression may not be confined to AH-NSCs within the SGZ. To address this point, we co-labelled sections with SOX2 and S100ß, a marker for astrocytes, or with the oligodendrocyte marker OLIG2. Quantification of co-labelled cells located within the SGZ revealed that less than 10% of the $SOX2^{+ve}$ cells in the

SGZ niche were S100ß-expressing cells of the astrocyte lineage, whereas less than 3% of the SOX2^{+ve} cells were immunopositive for OLIG2. As such, the majority of cells expressing high levels of SOX2 within the SGZ are likely to be AH-NSCs. Secondly, we measured nuclear size. Consistent with previous observations that NSCs are comparatively large (Rietze et al., 2001), the average area of the nucleus of dividing TBR2^{-ve} cells was approximately two-fold larger than Ki67^{+ve}; TBR2^{+ve} cells (Figure 2A, C; $P < 0.001$). Finally, if dividing TBR2^{-ve} cells are AH-NSCs then we would expect that some of these cells, except for those that were horizontally orientated or out of focal plane (Lugert et al., 2010), to have a radial GFAP^{+ve} process. We investigated this by staining for Ki67, TBR2 and GFAP and observed that indeed many of the dividing TBR2^{-ve} cells were clearly linked to a radial GFAP^{+ve} process (Figure 2D, D'). Together these data suggest that a significant proportion of dividing TBR2^{-ve} cells are AH-NSCs.

Ki67^{+ve}; TBR2$^{–ve}$ cells include horizontal AH-NSCs

Are all dividing TBR2^{-ve} cells in the SGZ AH-NSCs? Or does some fraction of these cells have another identity? For example, could some dividing, TBR2^{-ve} cells be IPs that do not express TBR2? To address this, we stained *Hes5*::GFP mice with Ki67 and TBR2, predicting that if dividing TBR2^{-ve} cells were AH-NSCs they should report high notch activity, which is indicated by GFP fluorescence in this line (Basak and Taylor, 2007; Lugert et al., 2010). Significantly, we found that all of the dividing, TBR2^{-ve} cells analysed expressed GFP (24/24 cells) (Figure 3A-C). This finding was confirmed via the analysis of a second marker of proliferation, PCNA, in the *Hes5*::GFP line, in which all of the PCNA$^{+ve;}$ TBR2^{-ve} cells expressed GFP (31/31 cells; Supplementary Figure 1). The co-localisation of GFP with all of the dividing, TBR2^{-ve} cells suggests that this population consists of AH-NSCs.

The advantage of the nuclear-only stain described here is that it should enable the identification of dividing AH-NSCs regardless of their orientation. The findings of Lugert and colleagues (2010) revealed that up to two-thirds of dividing AH-NSCs, as defined by *Hes5::*GFP expression, are in a horizontal orientation, while only the remaining third were the classic radially-orientated AH-NSCs. To test whether the dividing TBR2^{-ve} population included both horizontal and radial cells we stained for Ki67 and TBR2 in *Hes5*::GFP mice, and used the cytoplasmic GFP label to examine

cellular morphology. We found that approximately half the dividing TBR2^{-ve} cells exhibited a classical radial process (54%, 13/24 cells) (Figure 3A, D), while the remaining GFP^{+ve}; TBR2^{-ve} cells exhibited only a short horizontal process, fitting the description of horizontal AH-NSCs by Lugert and colleagues (2010) (46%, 11/24 cells) (Figure 3B, D). Together these data demonstrate that dividing TBR2^{-ve} cells, represent a population of AH-NSCs that includes cells with both radial and horizontal morphology.

Discussion

This study provides a morphology independent approach to identify dividing AH-NSCs. The significance of this study, apart from it's accuracy and simplicity, lies in the fact that the majority of quantification methods for AH-NSCs do not account for the putative population of horizontal AH-NSCs, as they do not possess a radially orientated fibre. While the true lineage potential and self-renewing capacity of horizontal AH-NSCs is yet to be established, they potentially account for at least half (this study) or two-thirds (Lugert et al., 2010; Jhaveri et al., 2015) of the dividing precursor pool in the dentate gyrus that express stem-cell specific markers and characteristics (e.g. $SOX2^{high}$, *Hes5*::GFP^{+ve}, $TBR2^{-ve}$). Assuming these horizontal cells are *bone fide* NSCs, current methods would underestimate stem cell numbers, or misrepresent these horizontal cells as IPs. This is particularly important, as scenarios exist where the enhancement or inhibition of certain signalling pathways may have no effect on the relative activation of radial AH-NSCs but could affect the activation of horizontal cells. Current quantification methods would miss these effects. Indeed, there is evidence that subpopulations of AH-NSCs respond differently to signalling cues. For example, reporter strains such as the *Hes5*::GFP and *nestin*::GFP lines have previously been used in conjunction with the expression of EGFR to isolate homogeneous populations of neurosphere forming precursors *in vitro* which contain distinct subpopulations that are responsive to norepinephrine exposure or KCl-depolarisation (Jhaveri et al., 2015).

There are other advantages to the method described here. For example, because the protocol only uses nuclear-localised antigens, it can be used to quickly quantify dividing AH-NSCs either manually or in an automated manner using image analysis software. This is in stark contrast to the current method that requires users to trace a radial process back to the correct nucleus in the SGZ, which is both time-consuming and difficult to automate. Our approach is also likely to be more accurate. Dividing neural progenitors are often found in cellular clusters (Hodge et al., 2008), and it becomes difficult to trace a radial process back to the correct nucleus. Moreover, because our method relies only on the co-localisation of two nuclear antigens, a relatively low-resolution confocal image is sufficient for the correct identification of these cells. Lastly, our method requires only a dual antibody stain (Ki67 and TBR2).

Combining this stain with other markers can provide additional information if required. For example, a triple-stain with GFAP would provide an estimate of the proportion of dividing AH-NSCs that are radial ($GFAP^{+ve}$ radial process) or horizontally orientated. Alternately, a triple stain with SOX2 could be used to also estimate the number of quiescent AH-NSCs ($Ki67^{-ve}$; $SOX2^{+ve}$; $TBR2^{-ve}$). Importantly, there are caveats to this method. For example, although we confine our analysis to the SGZ of the dentate gyrus, we cannot rule out that $Ki67^{+ve}$; $TBR2^{-ve}$ are not dividing oligodendrocyte precursors or microglia with only these two stains. That said, our analysis of SOX2 expression revealed that less than 3% of $SOX2^{+ve}$ cells within the SGZ co-expressed the oligodendrocyte marker OLIG2, suggesting that the vast majority of these cells are AH-NSCs. Furthermore, triple labelling with cell-type specific markers can be used to quickly determine the percentage of $Ki67^{+ve}$; $TBR2^{-ve}$ that are not AH-NSCs, and whether the proportion of these cells changes during different experimental conditions or during aging.

Despite such caveats, the simple morphology independent approach to identify dividing AH-NSCs described in this study is an improvement over existing methods because it allows for the rapid and accurate quantification of dividing AH-NSCs. Critically, it is inclusive of horizontally-orientated cells that traditional quantifications methods ignore. While further work is needed to establish the true identity and fate potential of horizontally-orientated precursors in the dentate gyrus, our method will be pivotal to provide a comprehensive interpretation of changes to precursor cell numbers in studies that investigate the molecular control of neurogenesis.

Experimental Procedures

Animal ethics

The work performed in this study conformed to The University of Queensland's Animal Welfare Unit Guidelines for Animal Use in Research (AEC approval numbers QBI/353/13/NHMRC and QBI/355/13/NHMRC/BREED). All experiments were performed in accordance with the Australian Code of Practice for the Care and Use of Animals for Scientific Purposes, and were carried out in accordance with The University of Queensland Institutional Biosafety Committee.

Animals

Two mouse lines were used in this study, wild-type C57BL/6J mice, and *Hes5::*GFP mice (CD1 background) (Basak and Taylor, 2007; Lugert et al., 2010). These mice contain a 3 kilobase (kb) portion of *Hes5* gene regulatory elements (1.6 kb upstream of the transcriptional start site, 1.4 kb downstream) controlling the expression of GFP. All mice in this study were analysed between 12-16 weeks of age. Both male and female mice were used.

Primary antibodies

The rabbit primary antibodies used in this study were anti-GFAP (Z033429-2, 1/1000, Dako), anti-TBR2 (ab23345, 1/800, Abcam) or monoclonal anti-TBR2 (EPR19012, 1/200, Abcam); the mouse primary antibodies were anti-Ki67 (550609, 1/200, BD Pharmingen), mouse anti-PCNA (ab29, 1/100, Abcam) and mouse anti-GFAP (MAB 360, 1/500, Millipore, MA); the rat primary was anti-Ki67 FITC clone SolA15 (11-5698-80 1/400, San Diego, CA); the goat primary was anti-DCX (sc-8066, 1/200, Santa Cruz), and chicken primary was anti-GFP (ab13970, 1/500, Abcam).

Tissue processing and immunofluorescence

Animals were perfused transcardially with phosphate buffered saline (PBS) followed by 4% (w/v) paraformaldehyde in PBS. The dorsal skull of animals was removed and brains were post-fixed for 1-2 weeks. Coronal brain sections were cut with a Vibratome (Leica, Deerfield, IL) at a thickness of 50 µm.

Prior to immunostaining, sections were mounted on Superfrost slides. Heat-mediated antigen retrieval was then performed in 10 mM sodium-citrate solution in PBS (pH 6.0) at 95°C for 15 min. Exceptions to this protocol were *Hes5*::GFP sections, in which heat-mediated antigen retrieval was performed for only 2 min. This shorter retrieval was required so as to not irreversibly damage the GFP epitope (Nakamura et al., 2008). A standard immunofluorescence protocol was then performed as described previously (Harris et al., 2016a).

Microscopy and image processing

Confocal images were acquired as 1 µm optical sections spanning a 10 µm thick z-stack on a Zeiss inverted Axio-Observer fitted with a W1 Yokogawa spinning disk module and Hamamatsu Flash4.0 sCMOS camera and Slidebook software (3i). Image channels were pseudocolored to allow for overlay, cropped, and minimum and maximum grey values were adjusted in ImageJ (freeware). Individual images were resized in Photoshop (Adobe), and image tiles were constructed as display items in Illustrator (Adobe). The quantification of immunopositive cells from these images was restricted the SGZ, which we defined as 2 cell widths above and below the innermost granule cell of the dentate gyrus.

Fluorescence intensity quantification

A single in focus plane was used to quantify SOX2 fluorescence. An outline was drawn around each cell nuclei using the DAPI channel and the area, mean grey value and integrated density were measured (ImageJ). The total corrected cellular fluorescence (TCCF) = integrated density – (area of selected cell * mean fluorescence of background readings) was then calculated (McCloy et al., 2014).

Statistics

Student's *t*-tests were performed in Graphpad Prism (7.0) to compare the relative SOX2 fluorescence intensity (TCCF) and nuclei area of $Ki67^{+ve}$ $TBR2^{-ve}$ and $Ki67^{+ve}$ $TBR2^{+ve}$ cells. Data was obtained from at least 5 cells from each individual mouse (n = 3). Because we were interested in variability between cells within the SGZ niche, each individual cell was considered a biological replicate. This approach allows for a better measure of the biological variability per cell, rather than when averaging the values from multiple cells per mouse.

Acknowledgements

We thank Prof. Perry Bartlett for the provision of the *Hes5*::GFP mice. Microscopy was performed in the Queensland Brain Institute's Advanced Microscopy Facility. This work was supported by an Australian Research Council grant (DP160100368 to MP). MP was supported by a fellowship (Australian Research Council Future Fellowship; FT120100170) and DJJ was supported by Mater Foundation Fellowship. LH and SO were supported by Australian Postgraduate Awards.

References

Akers KG, Martinez-Canabal A, Restivo L, Yiu AP, De Cristofaro A, Hsiang HL, Wheeler AL, Guskjolen A, Niibori Y, Shoji H, Ohira K, Richards BA, Miyakawa T, Josselyn SA, Frankland PW. 2014. Hippocampal neurogenesis regulates forgetting during adulthood and infancy. Science 344:598-602.

Andersen J, Urban N, Achimastou A, Ito A, Simic M, Ullom K, Martynoga B, Lebel M, Goritz C, Frisen J, Nakafuku M, Guillemot F. 2014. A transcriptional mechanism integrating inputs from extracellular signals to activate hippocampal stem cells. Neuron 83:1085-1097.

Andreu Z, Khan MA, Gonzalez-Gomez P, Negueruela S, Hortiguela R, San Emeterio J, Ferron SR, Martinez G, Vidal A, Farinas I, Lie DC, Mira H. 2015. The cyclin-dependent kinase inhibitor p27 kip1 regulates radial stem cell quiescence and neurogenesis in the adult hippocampus. Stem Cells 33:219-229.

Basak O, Taylor V. 2007. Identification of self-replicating multipotent progenitors in the embryonic nervous system by high Notch activity and Hes5 expression. Eur J Neurosci 25:1006-1022.

Bergmann O, Spalding KL, Frisen J. 2015. Adult Neurogenesis in Humans. Cold Spring Harb Perspect Biol 7:a018994.

Braun SM, Pilz GA, Machado RA, Moss J, Becher B, Toni N, Jessberger S. 2015. Programming Hippocampal Neural Stem/Progenitor Cells into Oligodendrocytes Enhances Remyelination in the Adult Brain after Injury. Cell Rep 11:1679-1685.

Castro DS, Martynoga B, Parras C, Ramesh V, Pacary E, Johnston C, Drechsel D, Lebel-Potter M, Garcia LG, Hunt C, Dolle D, Bithell A, Ettwiller L, Buckley N, Guillemot F. 2011. A novel function of the proneural factor Ascl1 in progenitor proliferation identified by genome-wide characterization of its targets. Genes Dev 25:930-945.

Cuylen S, Blaukopf C, Politi AZ, Muller-Reichert T, Neumann B, Poser I, Ellenberg J, Hyman AA, Gerlich DW. 2016. Ki-67 acts as a biological surfactant to disperse mitotic chromosomes. Nature 535:308-312.

Endl E, Gerdes J. 2000. The Ki-67 protein: fascinating forms and an unknown function. Experimental Cell Research 257: 231-237.

Ernst A, Frisen J. 2015. Adult neurogenesis in humans- common and unique traits in mammals. PLoS Biol 13:e1002045.

Gerdes J, Schwab U, Lemke H, Stein H. 1983. Production of a mouse monoclonal antibody reactive with a human nuclear antigen associated with cell proliferation. International Journal of Cancer 31: 13-20.

Goncalves JT, Schafer ST, Gage FH. 2016. Adult Neurogenesis in the Hippocampus: From Stem Cells to Behavior. Cell 167:897-914.

Guillemot F, Hassan BA. 2016. Beyond proneural: emerging functions and regulations of proneural proteins. Curr Opin Neurobiol 42:93-101.

Gulbins E, Palmada M, Reichel M, Luth A, Bohmer C, Amato D, Muller CP, Tischbirek CH, Groemer TW, Tabatabai G, Becker KA, Tripal P, Staedtler S, Ackermann TF, van Brederode J, Alzheimer C, Weller M, Lang UE, Kleuser B, Grassme H, Kornhuber J. 2013. Acid sphingomyelinase-ceramide system mediates effects of antidepressant drugs. Nat Med 19:934-938.

Harris L, Zalucki O, Gobius I, McDonald H, Osinki J, Harvey TJ, Essebier A, Vidovic D, Gladwyn-Ng I, Burne TH, Heng JI, Richards LJ, Gronostajski RM, Piper M. 2016a. Transcriptional regulation of intermediate progenitor cell generation during hippocampal development. Development 143:4620-4630.

Harris L, Zalucki O, Piper M, Heng JI. 2016b. Insights into the Biology and Therapeutic Applications of Neural Stem Cells. Stem Cells Int 2016:9745315.

Hodge RD, Kowalczyk TD, Wolf SA, Encinas JM, Rippey C, Enikolopov G, Kempermann G, Hevner RF. 2008. Intermediate progenitors in adult hippocampal neurogenesis: Tbr2 expression and coordinate regulation of neuronal output. J Neurosci 28:3707-3717.

Hodge RD, Nelson BR, Kahoud RJ, Yang R, Mussar KE, Reiner SL, Hevner RF. 2012. Tbr2 is essential for hippocampal lineage progression from neural stem cells to intermediate progenitors and neurons. J Neurosci 32:6275-6287.

Hussaini SM, Jun H, Cho CH, Kim HJ, Kim WR, Jang MH. 2013. Heat-induced antigen retrieval: an effective method to detect and identify progenitor cell types during adult hippocampal neurogenesis. J Vis Exp.

Jhaveri DJ, Mackay EW, Hamlin AS, Marathe SV, Nandam LS, Vaidya VA, Bartlett PF. 2010. Norepinephrine directly activates adult hippocampal precursors via beta3-adrenergic receptors. J Neurosci 30:2795-2806.

Jhaveri DJ, O'Keeffe I, Robinson GJ, Zhao QY, Zhang ZH, Nink V, Narayanan RK, Osborne GW, Wray NR, Bartlett PF. 2015. Purification of neural precursor cells reveals the presence of distinct, stimulus-specific subpopulations of quiescent precursors in the adult mouse hippocampus. J Neurosci 35:8132-8144.

Kandasamy M, Lehner B, Kraus S, Sander PR, Marschallinger J, Rivera FJ, Trumbach D, Ueberham U, Reitsamer HA, Strauss O, Bogdahn U, Couillard-Despres S, Aigner L. 2014. TGF-beta signalling in the adult neurogenic niche promotes stem cell quiescence as well as generation of new neurons. J Cell Mol Med 18:1444-1459.

Kim EJ, Ables JL, Dickel LK, Eisch AJ, Johnson JE. 2011. Ascl1 (Mash1) defines cells with long-term neurogenic potential in subgranular and subventricular zones in adult mouse brain. PLoS One 6:e18472.

Li G, Fang L, Fernandez G, Pleasure SJ. 2013. The ventral hippocampus is the embryonic origin for adult neural stem cells in the dentate gyrus. Neuron 78:658-672.

Lugert S, Basak O, Knuckles P, Haussler U, Fabel K, Gotz M, Haas CA, Kempermann G, Taylor V, Giachino C. 2010. Quiescent and active hippocampal neural stem cells with distinct morphologies respond selectively to physiological and pathological stimuli and aging. Cell Stem Cell 6:445-456.

Lugert S, Vogt M, Tchorz JS, Muller M, Giachino C, Taylor V. 2012. Homeostatic neurogenesis in the adult hippocampus does not involve amplification of Ascl1(high) intermediate progenitors. Nat Commun 3:670.

Martynoga B, Mateo JL, Zhou B, Andersen J, Achimastou A, Urban N, van den Berg D, Georgopoulou D, Hadjur S, Wittbrodt J, Ettwiller L, Piper M, Gronostajski RM, Guillemot F. 2013. Epigenomic enhancer annotation reveals a key role for NFIX in neural stem cell quiescence. Genes Dev 27:1769-1786.

McCloy RA, Rogers S, Caldon CE, Lorca T, Castro A, Burgess A. 2014. Partial inhibition of Cdk1 in G 2 phase overrides the SAC and decouples mitotic events. Cell Cycle 13:1400-1412.

Nakamura KC, Kameda H, Koshimizu Y, Yanagawa Y, Kaneko T. 2008. Production and histological application of affinity-purified antibodies to heat-denatured green fluorescent protein. J Histochem Cytochem 56:647-657.
Nicola Z, Fabel K, Kempermann G. 2015. Development of the adult neurogenic niche in the hippocampus of mice. Front Neuroanat 9:53.
Rietze RL, Valcanis H, Brooker GF, Thomas T, Voss AK, Bartlett PF. 2001. Purification of a pluripotent neural stem cell from the adult mouse brain. Nature 412:736-739.
Scholzen T, Gerdes J. 2000. The Ki-67 protein: from the known and the unknown. J Cell Physiol 182:311-322.
Shin J, Berg DA, Zhu Y, Shin JY, Song J, Bonaguidi MA, Enikolopov G, Nauen DW, Christian KM, Ming GL, Song H. 2015. Single-Cell RNA-Seq with Waterfall Reveals Molecular Cascades underlying Adult Neurogenesis. Cell Stem Cell 17:360-372.
Spalding KL, Bergmann O, Alkass K, Bernard S, Salehpour M, Huttner HB, Bostrom E, Westerlund I, Vial C, Buchholz BA, Possnert G, Mash DC, Druid H, Frisen J. 2013. Dynamics of hippocampal neurogenesis in adult humans. Cell 153:1219-1227.
Urban N, van den Berg DL, Forget A, Andersen J, Demmers JA, Hunt C, Ayrault O, Guillemot F. 2016. Return to quiescence of mouse neural stem cells by degradation of a proactivation protein. Science 353:292-295.
von Bohlen und Halbach O. 2011. Immunohistological markers for proliferative events, gliogenesis, and neurogenesis within the adult hippocampus. Cell Tissue Res 345:1-19.
Yousef H, Morgenthaler A, Schlesinger C, Bugaj L, Conboy IM, Schaffer DV. 2015. Age-Associated Increase in BMP Signaling Inhibits Hippocampal Neurogenesis. Stem Cells 33:1577-1588.
Yun S, Reynolds RP, Masiulis I, Eisch AJ. 2016. Re-evaluating the link between neuropsychiatric disorders and dysregulated adult neurogenesis. Nat Med 22:1239-1247.

Figure legends

Figure 1: Negative selection against TBR2 is sufficient to exclude dividing IPs and neuroblasts

(**A**) Coronal section of an adult mouse brain at the level of the hippocampus stained for DAPI (white). (**B**) A schematic showing the dividing (Ki67^{+ve}) cell types in the adult hippocampus. (**C, E**) The same coronal section as in (**A**) showing channels for (**in C**) TBR2 (blue), Ki67 (magenta) or (**in E**) TBR2, Ki67 and DCX (**green**). Boxed regions in **C** and **E** are presented in **C'** and **E'** respectively. (**D**) The majority of TBR2^{+ve} cells (arrows in **C'**) co-labelled with Ki67. Surprisingly, all dividing DCX^{+ve} neuroblasts also expressed TBR2 (arrowheads in **E'**), as quantified in (**F**). Scale bar (in **A**): **A**, **C**, **E** = 168 µm; **C'**, **E'** = 22.5 µm.

Figure 2: Ki67^{+ve}; TBR2^{-ve} nuclei have AH-NSC characteristics

(A-A") Coronal section of an adult mouse brain at the level of the hippocampus, showing DAPI (white, **A**), SOX2 (green, **A'**) TBR2 (blue, **A''**) and Ki67 (magenta, **A''**) staining. The dashed lines demarcate the SGZ of the dentate gyrus. Ki67^{+ve}; TBR2^{-ve} cells (e.g. arrowhead in **A**) have higher SOX2 fluorescence (**A', B**) and relatively larger nuclei (**A-A", C**) than Ki67^{+ve}; TBR2^{+ve} cells (arrows in **A-A"**). (**D, D'**) Coronal section of an adult mouse hippocampus showing TBR2 (blue, **D**), GFAP (red, **D** and **D'**) and Ki67 (magenta, **D'**) staining. Many Ki67^{+ve}; TBR2^{-ve} cells (arrowhead) were linked to a radial GFAP^{+ve} process (arrows). ***P < 0.001, t-test. Scale bar (in **A)**: 9 µm.

Figure 3: Ki67^{+ve}; TBR2^{-ve} nuclei include horizontally orientated *Hes5::*GFP AH-NSCs

(A-A"', B-B"') Coronal section of a mouse hippocampus, showing the dentate gyrus, with *Hes5::*GFP in (green), Ki67 (magenta) and TBR2 (red). (**A-A"'**) Some Ki67^{+ve}; TBR2^{-ve} nuclei (arrowhead) had a radial morphology (arrows), while others (**B-B"'**) had a horizontal morphology (arrowheads). **(C)** All Ki67^{+ve}; TBR2^{-ve} nuclei expressed GFP. (**D**) Radial and horizontal Ki67^{+ve}; TBR2^{-ve} nuclei were present in approximately equal numbers. Scale bar (in **A**): 17 µm.

Figures

Figure 1

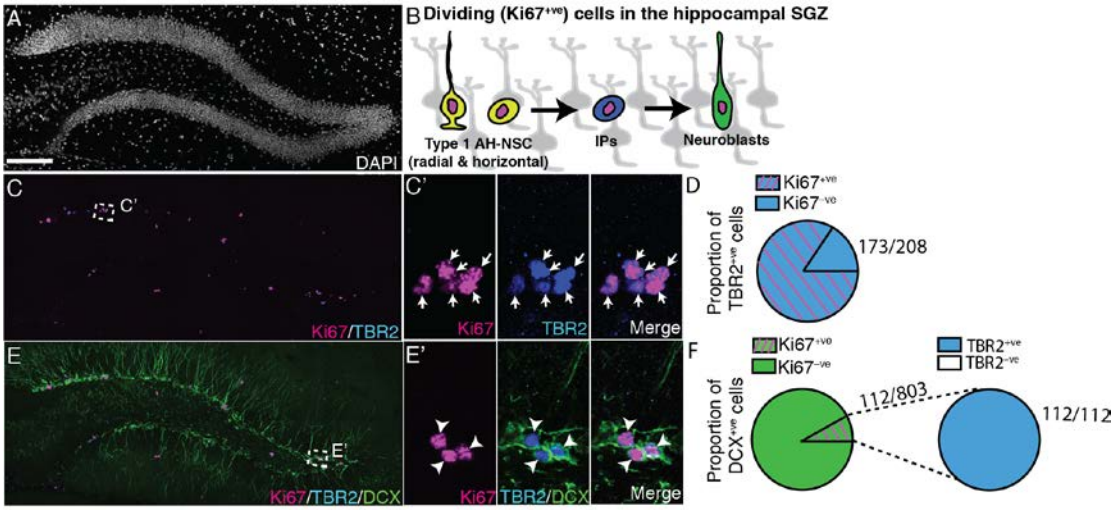

Figure 2

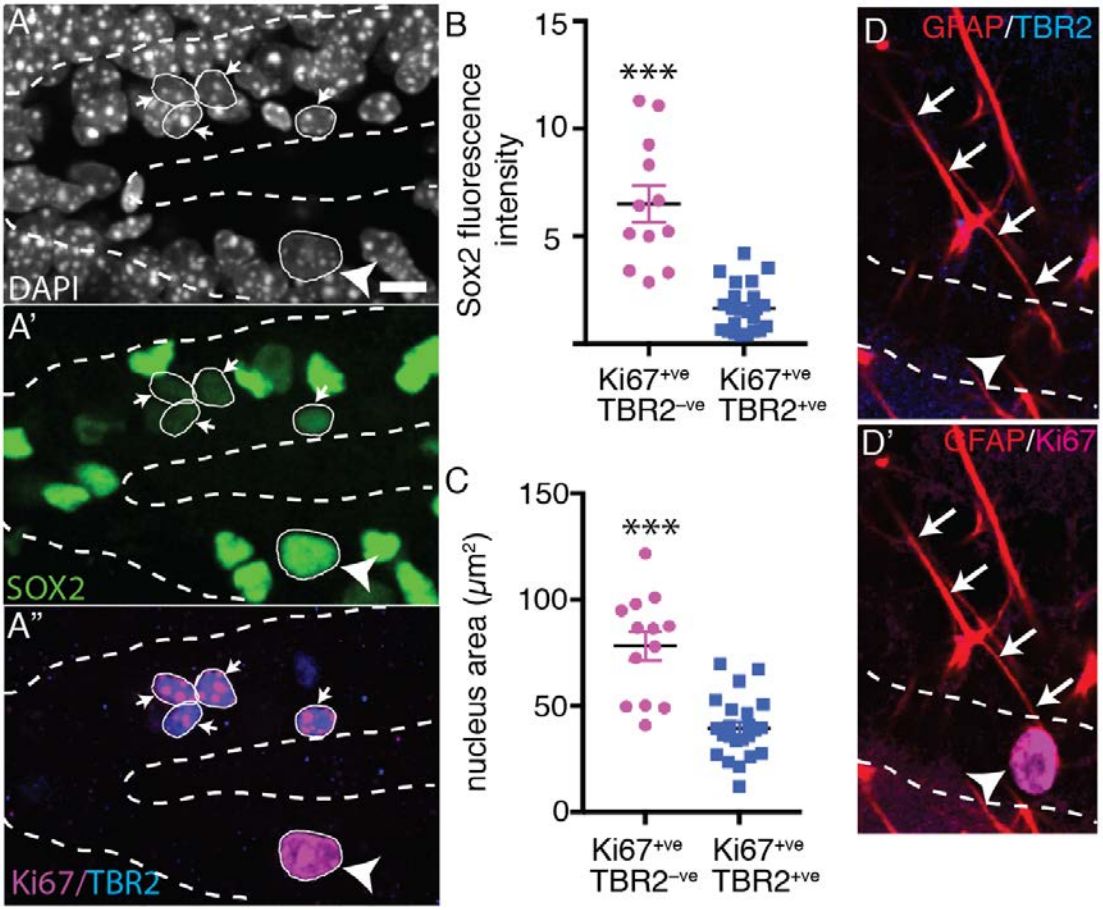
A
DAPI
A'
SOX2
A"
Ki67/TBR2
B
Sox2 fluorescence intensity
15
10
5
***
Ki67+ve TBR2−ve
Ki67+ve TBR2+ve
C
nucleus area (μm²)
150
100
50
0
***
Ki67+ve TBR2−ve
Ki67+ve TBR2+ve
D
GFAP/TBR2
D'
GFAP/Ki67

Figure 3

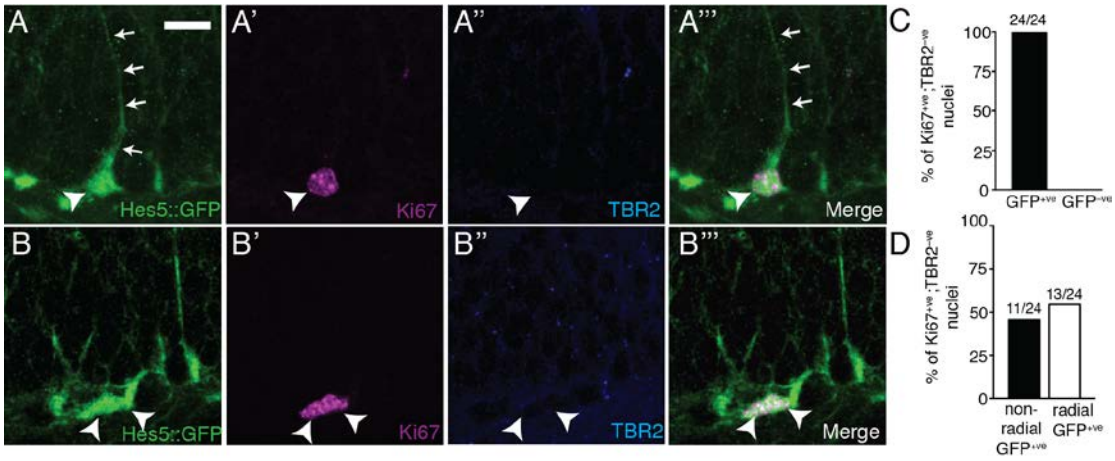
A
A'
A''
A'''
Hes5::GFP
Ki67
TBR2
Merge
B
B'
B''
B'''
Hes5::GFP
Ki67
TBR2
Merge
C
% of Ki67+ve;TBR2-ve nuclei
24/24
100
75
50
25
0
GFP+ve
GFP-ve
D
% of Ki67+ve;TBR2-ve nuclei
11/24
13/24
100
75
50
25
0
non-radial GFP+ve
radial GFP+ve